Structural stability of belite sulfoaluminate clinkering polymorphs

M. Laanaiya, A. Bouibes, Ali Zaoui

Version of Record: https://www.sciencedirect.com/science/article/pii/S0167273821000941
Manuscript_9770f5696b4a118da99e5938ad13b1d5

Structural stability of belite sulfoaluminate clinkering polymorphs

M. Laanaiya, A. Bouibes and A. Zaoui*
Univ. Lille, IMT Lille Douai, Univ. Artois, JUNIA, ULR 4515 - LGCgE, Laboratoire de Génie Civil et géo-Environnement, F-59000 Lille, France

Abstract

Belite is a major phase of cement clinker that has attracted great attention due to its applicability in the production of environmental friendly cement. In this work, we investigate and compare properties of γ- β- polymorphic forms of belite. γ-belite is the ground state phase. Whereas, β-belite is found to be metastable phase of belite and it is the most present phase of belite in ordinary cement. γ-belite is a non-reactive phase with water of belite; while β-belite clearly reacts with water. First-principles methods based on Density Functional Theory within the pseudopotential formalism have been used here to study the structural, mechanical and electronic properties of both belite phases. The influence of the crystallographic structure of belite on the reactive sites distribution under nucleophilic and electrophilic attacks has been highlighted. In addition, a noticeable difference of the reactive sites localisation of the two phases has been pointed out. Our results are in agreement with the observed high-water reactivity of β-belite compared to γ-belite. However, our calculations show very slight effect of the belite polymorphism on mechanical properties. In particular, the elastic behaviour of γ- and β-belite shows important similarities regarding the elastic parameters obtained for the two belite phases. Nevertheless, our results predict the γ-belite to be slightly more rigid and resistant to mechanical loading compared to β-belite.

Keywords: Belite; DFT; Phase stabilities; Mechanical properties; Water reactions.

*Email address: azaoui@polytech-lille.fr

I. Introduction

Belite, or Dicalcium Silicate, has been the focus of attention for producing environmentally friendly cements. Belite requires a lower energy synthesis and has a low limestone demand compared to alite, the first major component of ordinary Portland cement (OPC). In fact, the fabrication of high belite cements can reduce up to 35% CO_2 emission than ordinary cement [1]. Belite Sulfoaluminate (BSA) belite-rich cements have been proposed as an alternative building material to alite-rich OPC, where a part of calcite is substituted by calcium sulphate in BSA leading to less calcite demand compared to OPC [2]. BSA cements are produced by mixing limestone, Kaolin, bauxite and gypsum required for the formation of the BSA major phases: belite C_2S (C=CaO, S=SiO_2) with more than 50% wt. content, Ye'elimite $C_4A_3\bar{S}$ (A=Al_2O_3, $\bar{S}$ =SO_3), responsible for early-age strength development instead of alite C_3S, and C_4AF (F=F_2O_3) [3]. Unfortunately, the slow hydration mechanism of belite leads to a slower development of belite rich cement strength. Several studies have been conducted on improving belite's reactivity. Belite C_2S has a sequence of five polymorphs: γ- C_2S, β-C_2S, α'$_L$-C_2S, α'$_H$-C_2S and α-C_2S [4-5]. When increasing the temperature at room pressure, the structure follows the phase transitions sequence: γ → α'$_L$→ α'$_H$→α [6]. On the cooling path, the β- C_2S metastable phase appears below 675°C between α'$_L$ and γ-phase [7]. γ-belite with the orthorhombic olivine structure (space group: Pbnm) is the thermodynamically stable phase at room temperature. γ-belite is almost nonreactive with water [8]. The metastable β phase of belite with a monoclinic phase (space group: P21/n) stabilized at room temperature conditions exhibits higher reactivity rate with water at room temperature. β-phase is the predominant form of belite in normal portlandite cement. The incorporation of small amounts at levels lower than 2% of sulfur trioxide SO_3 in cement clinker leads to the stabilization of β-belite [9]. Studies on chemistry stabilization based on ionic properties have shown that the addition of impurity ions such as S^{6+}, B^{3+}, P^{5+}, Cr^{6+}, As^{5+} and V^{5+} effectively stabilize the β-phase of belite [10]. The other belite phases α'$_L$, α'$_H$ and α are stable at higher temperature. Recently, the order of phase transitions and phonon dynamics of belite were studied using DFT calculations and interatomic potential functions [11]. Chemical stabilization of reactive β-form of belite down to

room temperature by incorporating guest ions has been investigated [12, 13] and many experimental works tried to examine the polymorphism-reactivity dependence [14]. However, the reactivity mechanism of the different belite phases is not well understood due to experiment limitations and inconsistencies between theoretical predictions and experimental data [15]. In addition, considering the low synthesis temperature of gamma-polymorph compared to β-polymorph makes a reactive version of γ-belite widely chased from the environmental perspective [16]. Therefore, studying the influence of the crystallography of belite phases on reactivity is crucial to enhance its reactivity. Moreover, belite is responsible for developing late strength. Understanding the effect of the belite complex on cement cohesion and mechanical properties is quite important in the field of developing high performance concrete [17]. Atomistic simulations using first-principle and force field methods have demonstrated their great potential for studying cement complex phases [18-20]. In this work, we aim to investigate and to compare the properties of the belite ground-state phase: γ-phase, as well as the most present form of belite in traditional cements, i.e. β-phase, by means of first-principles calculations in order to capture the reactivity features of cement belite.

II. Computational details

We have performed DFT (Density Functional Theory) calculations on γ- and β- belite using the Vienna *ab initio* package (VASP) [21, 22]. The Projected Augmented Wave (PAW) [23] method was adopted with the Pseudopotential approach. The valence electron configuration O $2s^2$ $2p^4$, Si $3s^2$ $3p^2$ and Ca $3s^2$ $3p^6$ $4s^2$ have been used for the two belite phases. The Generalised Gradient approximation GGA [24] with PBE (Perdew-Burke-Ernzerhof) parameterisation [25] and the Local density approximation LDA [26] were both selected to evaluate the exchange-correlation effects and to test the functional dependence of our results. The convergence of total energies was amply reached with respect of cut-off energy of 600 eV for the three functionals. Well converged meshes of 9x4x7 and 8x7x5 using Monkhorst-Pack method [27] were chosen to sample the first Brouillon-zone for γ-belite and β-belite respectively. Geometry optimisation was achieved through conjugate-Gradient (cg) energy minimization algorithm with a stopping criterion of 10^{-7} eV. In addition, *ab initio* molecular dynamics simulations (AIMD) were performed for 2x2x2 supercells of each of γ- and β- phases at 300°K of temperature. The AIMD simulations were executed during 50 fs with a time step of 0.5 fs. The AIMD trajectory was analysed using VMD program in order to plot the radial pair distribution function [28].

III. Results and discussions

1-Structural properties

The initial structure of γ-belite (space group: Pbnm) was set up based on Smith et al. experimental data [29] and β-belite initial structure (space group: P21/n) was taken from Tsurumu et al. work [30]. The unit cells of both γ- and β-belite consist of 16 oxygen atoms, 8 calcium atoms and 4 silicon atoms (4[Ca_2SiO_4]) and the Wyckoff positions are given in Table 1. The unit cells of initial structures are illustrated in Figure.1

The structures were completely relaxed from each functional. For a given set of lattice constants, total energies are computed by means of LDA and GGA. The equilibrium bulk modulus (B_0) and its pressure derivative (B_0') have been determined by fitting the obtained energy data with respect to volume using the Murnaghan equation of state EOS [31]:

$$E(V) = E_0 + \frac{B_0.V}{B_0'}\left[\left(\frac{V_0}{V}\right)^{B_0'}.\frac{1}{B_0'-1}+1\right]-\frac{B_0.V_0}{B_0'-1} \quad (1)$$

Where E_0 and V_0 are respectively the equilibrium energy and volume at zero pressure.

The calculated equilibrium cell parameters, bulk modulus and its pressure derivate are given in Table 2 and are compared to previous experimental and theoretical data [32-36]. The two used functionals provide very comparative cell parameters values to experiment data. For γ-belite, the best agreement is found by GGA approximation for the calculation of lattice constants with a slight underestimation of the cell parameters by less than 1.5%. The computed bulk modulus is in good agreement with previous theoretical studies. For β-belite, GGA slightly overestimates the lattice constants (less than 1.3%) in opposition to LDA with less than 1.9% underestimation of lattice constants. The calculated bulk modulus is in great agreement with theoretical available data and the found values by the two functionals are very comparable (97.0 GPa from GGA and 104.7 GPa from LDA).

2-Mechanical properties

The γ-polymorph of belite has an orthorhombic crystal structure. The orthotropic materials are characterised by three symmetry planes. According to this crystal symmetry, the elasticity tensor has 9 non-zero independent constituents: C_{11}, C_{22}, C_{33}, C_{44}, C_{55}, C_{66}, C_{12}, C_{23}, C_{31}. The necessary and sufficient mechanical stability conditions, or the born generic stability criteria, of an unstressed orthorhombic crystal to be satisfied are the following [37]:

$$C_{11} > 0;\ C_{11}C_{22} > C^2_{12}$$

$$C_{11}C_{22}C_{33}+2C_{12}C_{13}C_{23}-C_{11}C^2_{23}-C_{22}C^2_{13}-C_{33}C^2_{12}>0$$

$$C_{44}>0;\ C_{55}>0;\ C_{66}>0 \qquad (2)$$

The β-polymorph of belite has a monoclinic crystal structure. According to this crystal symmetry, the elasticity tensor has 9 non-zero independent constituents: C_{11}, C_{22}, C_{33}, C_{44}, C_{55}, C_{66}, C_{12}, C_{23}, C_{31}, C_{54}, C_{61}, C_{62}, C_{64}. The necessary and sufficient mechanical stability conditions, or the born generic stability criteria, of an unstressed monoclinic crystal to be satisfied are the followings [38]:

$$C_{11},\ C_{22},\ C_{33},\ C_{44},\ C_{55},\ C_{66} >0$$

$$C_{11}+C_{22}+C_{33}+3(C_{12}+C_{23}+C_{31})>0$$

$$C_{22}C_{66}-C^2_{62}>0\ ;\ C_{44}C_{55}-C^2_{54}>0$$

$$C_{22}+C_{33}-2C_{23} >0$$

$$C_{33}(C_{22}C_{66}-C^2_{62})+2C_{23}C_{26}C_{26}-C^2_{23}C_{66}-C^2_{36}C_{22}>0$$

$$2[C_{16}C_{36}(C_{22}C_{13}-C_{12}C_{23})+C_{16}C_{26}(C_{33}C_{12}-C_{13}C_{23})+C_{36}C_{26}(C_{11}C_{23}-C_{12}C_{13})]-[C^2_{16}(C_{22}C_{33}-C^2_{23})+C^2_{36}(C_{11}C_{22}-C^2_{12})+C^2_{26}(C_{11}C_{33}-C^2_{23})+C_{66}.x]>0$$

$$\text{Where } x=C_{11}C_{22}C_{33}-C_{11}C^2_{23}-C_{22}C^2_{31}-C_{33}C^2_{12}+2C_{12}C_{23}C_{31} \qquad (3)$$

The calculated elastic constants by the three used functionals are listed in Table 3. In all cases, the obtained values satisfy the elasticity stability conditions. From the elastic coefficients, we have determined the elastic compliances S_{ij}. Then, the four well-known parameters to quantify the response of a material to various solicitations: the bulk modulus (K), shear modulus (G), Young modulus (E) and Poisson's ratio are derived from the Voigt–Reuss–Hill (VRH) approximation that establishes the connection between the elastic behaviour of an aggregate and a single crystal.

The true values of calculated moduli are proven to lay between the Reuss and Voigt

calculated values [39]. In the following formulas, V and R denote Voigt and Reuss bounds respectively.

$$K_R \le K \le K_V \text{ and } \; G_R \le G \le G_V \tag{4}$$

$$K_R = \frac{1}{S_{11}+S_{22}+S_{33}+2(S_{12}+S_{23}+S_{31})} \tag{5}$$

$$K_V = \frac{C_{11}+C_{22}+C_{33}+2(C_{12}+C_{23}+C_{31})}{9} \tag{6}$$

$$G_R = \frac{15}{4(S_{11}+S_{22}+S_{33})-4(S_{12}+S_{23}+S_{31})+3(S_{44}+S_{55}+S_{66})} \tag{7}$$

$$G_V = \frac{C_{11}+C_{22}+C_{33}-(C_{12}+C_{23}+C_{31})+3(C_{44}+C_{55}+C_{66})}{15} \tag{8}$$

The final values of bulk and shear moduli can be taken as the average of Voigt and Reuss bounds.

The average value of Young modulus E and Poisson's ratio can be obtained by substituting the mean calculated values of K and G in:

$$E = \frac{1}{\frac{1}{3G}+\frac{1}{9K}} \tag{9}$$

$$\nu = \frac{1}{2}\left(1-\frac{3G}{3K+G}\right) \tag{10}$$

To quantify the elastic anisotropy, we used the universal elastic anisotropy index A^u calculated from Voigt and Reuss bounds of K and G as follows [40]:

$$A^u = 5\frac{G^V}{G^R}+\frac{K^V}{K^R}-6 \ge 0 \tag{11}$$

A zero value of A^u refers to a locally isotropic single crystal. The larger the value of A^u, the larger the anisotropy

We present the previous listed parameters in Table 3 along with the experimental and

theoretical available data. Comparing values of C_{11}, C_{22} and C_{33}, both LDA and GGA functionals predict a higher compressibility in the second principal direction (0 1 0) of the γ-phase crystal. The highest obtained value of C_{22} in the case of β-structure suggests a great resistance to compressibility in the second direction (0 1 0). Almost equal C_{11} and C_{33} values for β-belite predict a comparable resistance to compressibility in the first and third directions. Now, comparing C_{11}, C_{55}, and C_{66}, the system has more resistance to shear solicitation along the (0 0 1) direction for γ-belite and along the (1 0 0) for the β-belite. Obtained values from both LDA and GGA functionals are fairly comparable for the γ-structure; whereas a functional dependence of the results in the case of β-structure is noticed. Only mechanical properties of β-belite have been experimentally determined, thus we consider the reference values for γ-belite to be those predicted by other theoretical previous studies. In the following analysis, we will focus on the calculated values from GGA as the obtained lattice parameters are the closest to the experiment compared to LDA functional. The calculated bulk modulus K for γ-belite (101.08 GPa) is in great agreement with the calculated values from Force field calculations 95.56 GPa by Wang et al. [16] and 93.1GPa by Rejmak et al. [11]. The calculated bulk modulus for β-belite is about 5% lower with a value of 95.73GPa. Theoretical results using molecular dynamics calculations are quite controversial comparing the results obtained for β-belite [11,16]. The calculated bulk modulus by Wang et al. for β-belite (125.8 GPa) using reactive forcefields method (REAX) is 48% higher than that calculated by Rejmak et al. using interatomic potential (IP) calculations (84.9 GPa).

Shear and Young moduli were also found to be very comparable for both phases with slightly lower value for β-belite (of about 5%). Again, for γ-belite, our results for shear modulus and Young modulus are in excellent agreement with force field studies [11, 16]. On the other hand, greater differences are observed for β-belite. Results of Wang et al. describe a stiffer material with a Young modulus of 153.62 GPa; whereas the opposite was found by Rejmak et al. with a value of only 106 GPa. These values somewhat deviate from the 130-140 GPa range set by experimental measurements for beta-phase [41, 42]. By contrast, our results (E=123.02 GPa) are fairly close to the

experiment with a slight underestimation of about 5%. Let us notice that for a non-isotropic material the calculated value of Young modulus strongly depends on the considered direction. Since the calculated value only corresponds to the average value, differences between results are rather due to the used averaging formulas. We obtain the same value of Poisson's ratio for γ-phase (0.29) in both phases, which is quite close to -phase's 0.3 obtained by experimental studies on β-belite [43]. The calculated anisotropy indexes corresponding to a non-zero value confirms the anisotropy nature of belite. A higher anisotropy trend is observed in β-belite with a higher anisotropy index of 0.44 compared to 0.29 as expected considering the more symmetrical structure of the γ-belite.

3-Bonding and electronic properties

To obtain structural details about the bonding features of γ- and β-belite, we have analysed the bond lengths in both belite structures. Figure 2 reports the radial pair distribution function of Ca--Si, Ca--O and Si--O in γ and β-belite. From Figure 2.a, we can see two similar peaks of Ca_γ--Si_γ radial pair distribution located at the distances of 2.95Å and 3.55Å respectively. However, peaks in β-belite of Ca_β--Si_β coordination are located at larger distances: the first peak is located at 3.05Å, the second peak is located at 3.35Å and the third one at 3.85Å. In Figure 2.b, the radial pair distribution of Si--O was localized at 1.64Å showing a strong covalent bonding character in both γ- and β-structures. In Figure 2.c, the Ca--O radial pair distribution in β-structure is more variable indicating a higher flexibility compared to the sharp Ca--O bond distribution of the rigid γ-belite structure. The first peak was located at 2.32Å in γ-structure, while it was located at a larger distance 2.47Å in β-structure. In addition, a second peak of Ca--O coordination at 2.67Å appeared only in β-structure. Such large bond lengths make the ionic bond weaker and easily broken under chemical attacks, which may explain the metastability of β-structure. Another main structural difference is related to the coordination number of CaOx polyhedral in the two belite polymorphs. In γ-belite, calcium atoms are symmetrically surrounded by

six oxygen atoms whereas β-belite has two types of calcium atoms: seven-coordinated and eight-coordinated Ca_β. In contrast with γ-belite, the asymmetry of calcium atoms coordination in β-belite was identified as an important factor of water reactivity in calcium silicates [44], which may also explain the reactivity differences between the γ- and β-belite. In the hydration process, under-coordinated calcium atoms are believed to associate with oxygen atoms Ow of the water molecule while one of the hydrogen atoms Hw forms a hydrogen bond with the nearest oxygen atoms from the silicate groups promoting the formation of the main cement hydration products C-S-H and $Ca(OH)_2$ [45-47].

To investigate the bonding character of γ- and β-belite, we have calculated the net charges of atoms from Bader [48] partitioning of charge density using GGA functional. We report the net charge of each atom type in Table 4. Looking at the calculated Bader charge of both phases, we can notice that the Bader charge of Si, as well as of Ca atoms, is almost equal in β- and γ- belite phases. Silicon atoms have an averaged charge of about +3.1|e| in both phases; whereas calcium atoms Ca_γ in γ-phase and Ca_β in β-phase have a Bader charge of +1.56|e| and +1.58|e| respectively. The Bader charges on oxygen atoms O_γ in γ-belite are also equally distributed with a Bader charge of about -1.55|e|. However, different Bader charges were obtained for O_β atoms showing that the oxygen atoms are not equivalent in β-belite. From Table 4, we can define two sets of O_β: O1-type and O2-type with averaged charge of -1.54|e| and -1.57|e| respectively.

For further understanding of the bonding characteristics of the two belite phases, the total DOS illustrating the contribution of each atom type (calcium, oxygen and silicon) is calculated from GGA functionals. We display in Figure 3 the total DOS obtained from GGA functional for both γ-, and β-belite. Adopting the same energy scale for γ- and β-belite in Figure 3, for both γ- and β-belite the upper DOS region of the valence region of below the Fermi level is mainly due to oxygen atoms contribution. In addition, we can notice a larger amplitude in the highest occupied molecular orbital

(HOMO) from β-oxygen contribution leading to a higher reactivity of O atoms in β-phase compared to γ-phase under an electrophilic attack. The partial DOS (PDOS) of Oxygen presented in Figure 4 shows that this part is derived from 2p orbitals. In contrast, the conduction part above the Fermi level is dominated by calcium contribution and more precisely by 3d states of calcium as illustrated in Figure 5. This result perfectly agrees with Wang et al. [16] work and confirms that belite reactivity is mainly due to 2p-O and 3d-Ca states. The total DOS in Figure 3 shows very small contribution of Si atoms to DOS and thus for belite hydration reactivity.

For a deeper understanding of the reactivity of belite phases, the local reactivity can be also qualitatively analysed by comparing the plotted local density of states (LDOS) of Conduction bottom Minimum (CBM) and Valence Band Maximum (VBM) in Figure 6 and Figure 7 respectively. Parr et al. [49,50] have developed the Fukui function as a local reactivity descriptor based on the frontier orbital theory providing a qualitative measure of the reactivity of a given system. We can see from Figure 6 that the LDOS of CBM is delocalized for both phases. Therefore, no peculiar reactive sites to nucleophilic attacks can be deduced from this analysis even though the CBM LDOS is distributed differently comparing γ- and β-belite. It is mainly dispersed in the regions between Ca and SiO_4 polyhedral in β belite; whereas it is symmetrically dispersed in the space between calcium atoms (Ca2-Ca4 and Ca1-Ca3) in γ-belite. On the other hand, the plotted VBM in Figure 7 shows that both LDOS are localised around the Oxygen atoms and thus more likely to undergo electrophilic attacks in agreement with the previous DOS analysis. The VBM LDOS is shared between most oxygen atoms in γ-belite. However, we can see that LDOS is highly localised around few oxygen atoms in β-belite, which are the O1-type defined in the Bader charge analysis. To understand the origin of such results, we have investigated the DOS contributions of O1 and O2 oxygen types in β-belite. Figure 9 shows clearly a larger amplitude in HOMO orbital with a spotted peak that exclusively arises from O1-type contribution, which could explain the high localization of LDOS on O1 oxygen as well as the difference in the previously calculated Bader charges of O1 and O2 oxygen types in β-belite. Our results concur with other works [51, 52] suggesting that

the initial step of reactions of β-belite is the proton transfer from water molecules to oxygen atoms of β-belite.

To get more insights into the chemical bonding and the charge transfer in each phase, we have plotted the charge density in Figure 9 and the 2D-map in Figure 10 in planes containing the three types of atom (Si, Ca and O) that we named P_g and P_b plane for γ-phase and β-phase respectively. We see that silicon atoms are tightly bounded to the closest oxygen atoms in both phases. The strong projected charge density between the oxygen and silicon ions indicates the strong covalent bonding character as it was shown in Figure 2. On the other hand, the charge density is not quite important between calcium and oxygen ions confirming again the high ionic character of Ca-O bond in γ-phase the two belite phases. Figure 10 reveals however a significant difference regarding the charge density distribution over the oxygen atoms. Figure 10.a shows a uniform distribution of the electron density over the four oxygen atoms in γ-belite whereas an asymmetric electronic density on the O1-Ca1-O11 pairs in β – belite as shown in Fig.10.b. The non-uniform electron density distribution in P_b plane where the calcium atom is coordinated to O1 and O2 oxygen types is consistent with the Bader charge analysis and LDOS localization confirming the different electronic environments around the two types of oxygen. Thus, our analysis suggests that the high reactivity of β-belite is due to the electron transfer from calcium atoms to the reactive oxygen atoms of O1-type in β-belite that undergo electrophilic attacks from water (of type H+) in the hydration process.

IV. Conclusion

The main aim of this work was to determine and compare between structural, mechanical, bonding and electronic properties of γ- and β-belite by means of DFT calculations. The calculated structural and mechanical properties by GGA functional were found to be in great agreement with the experiment. Comparable elastic

parameters and moduli were obtained for γ- and β-belite with slightly higher values for γ-belite predicting that γ-phase is insignificantly more rigid and resistant. On the other hand, the analysis of chemical bonding and electronic properties of the two phases reveals relevant distinctions that may explain the stability of γ-belite and the reactivity of β-belite in the hydration process. In β-belite, two oxygen atoms types (O1 and O2) were distinguished by analysing the atomic charges and the most occupied energy levels near the Fermi level in the PDOS of O-2p states; whereas γ-belite exhibits a high symmetry in the charge distribution over all oxygen atoms. The uniformly distributed LDOS of VBM may also explain the non-reactivity to water of γ-belite; while the highly located LDOS of VBM around O1-type oxygen atoms indicates high reactivity under electrophilic attacks. Many theoretical works attempted to introduce impurities to enhance the β-belite reactivity rate. By analogy with the localized nature of VBM around O1-type, localizing the CBM LDOS around some specific calcium atoms by doping mechanisms [53] would efficiently increase the reactivity of β-belite under nucleophilic attacks, and thus the overall reactivity with water.

Tables

Table 1: Wyckoff Positions of atoms in γ-belite and β-belite according to experimental studies [28,29].

γ-belite (28)					β-belite (29)				
Atom	x	y	z	Site	Atom	x	y	z	Site
Si	0.4272	0.0985	0.2500	4c	Si	0.2700	-0.2200	0.4140	4e
Ca1	0.0000	0.0000	0.0000	4a	Ca1	0.2300	0.3420	0.4310	4e
Ca2	-0.0116	0.2804	0.2500	4c	Ca2	0.2270	0.0000	-0.2940	4e
O1	-0.2623	0.0867	0.2500	4c	O1	0.2180	0.0090	0.4410	4e
O2	0.3020	-0.0421	0.2500	4c	O2	0.0290	-0.3240	0.369	4e
O3	0.2925	0.1633	0.0599	8d	O3	0.4600	-0.2600	0.3150	4e
					O4	0.3240	-0.3140	-0.4210	4e

Table 2: Calculated lattice constants (a_0, b_0 and c_0), cell angles (α, β and γ), bulk modulus (B) and its pressure derivative (B') of γ-belite and β-belite and compared to experimental and other theoretical data.

	γ -belite					β -belite			
	This work (GGA)	This work (LDA)	Expt.[32]	Previous theor. (GGA-PBE) [33]	Previous theor. (ReaxFF) [34]	This work (GGA)	This work (LDA)	Expt. [35]	Previous theor. [36]
a_0 (Å)	5.07	5.02	5.08	5.11	5.13	5.57	5.43	5.5	5.11
b_0 (Å)	11.19	10.98	11.23	11.33	11.17	6.82	6.65	6.76	11.33
c_0 (Å)	6.72	6.6	6.76	6.8	6.33	9.37	9.14	9.32	6.8
α	90°	90°	90°	90°	90°	90°	90°	90°	90°
β	90°	90°	90°	90°	90°	94.7°	95.4185°	94.1°	94°
γ	90°	90°	90°	90°	90°	90°	90°	90°	90°
B (GPa)	82.1	85.2			95.56	97.03	104.69		111
B'	2.13	3.48				3.56	4.15		

Table 3: Calculated elastic constants C_{ij}, Bulk modulus (B), isotropic shear modulus (G), Young's modulus (E), Poisson's ratio (ν) and Universal anisotropy index (A^U)

	γ-belite				β-belite				
	This work		Other works		This work		Other works		
	GGA	LDA	Reax FF [16]	IP [11]	GGA	LDA	Reax FF [16]	IP [11]	Exp.
C_{11} (GPa)	189.22	200.82			167.1	202.19			
C_{22} (GPa)	128.58	136.26			192.85	254.47			
C_{33}(GPa)	163.62	174.28			168.76	203.72			
C_{44}(GPa)	60.90	65.24			52.58	62.25			
C_{55}(GPa)	46.75	49.92			45.53	55.92			
C_{66}(GPa)	64.34	67.5			31.12	41.51			
C_{12}(GPa)	72.22	76.63			47.97	58.66			
C_{23}(GPa)	71.81	76.74			58.48	72.02			
C_{31}(GPa)	76.89	80.87			63.39	77.29			
C_{54} (GPa)	-	-			-4.76	8.01			
C_{61} (GPa)	-	-			-10.21	-1.6			
C_{62} (GPa)	-	-			0.95	2.68			
C_{63} (GPa)	-	-			-9.07	-12.47			
K (GPa)	101.08	107.31	95.56	93.1	95.73	119.02	125.8	84.9	
G (GPa)	50.51	53.66	48.58	50.8	47.84	59.78	59	41,1	
E (GPa)	129.89	137.98	124.7	129	123.02	153.62	153.1	106.2	130-140 [39,40]
N	0.29	0.29		0.27	0.29	0.28		0.30	0.30 [41]
A^U	0.29	0.29			0.44	0.41			

Table 4: Bader charge of γ and β-belite

Atoms	γ-belite	β-belite

Ca	+1,56	+1,57
Si	+3,09	+3,10
O1	-1,55	-1,54
O2		-1,57

Figures Caption

Fig. 1: Structure of (a) γ-belite and (b) β-belite.

Fig.2: Radial pair distribution functions g(r) of calcium-silicon (a), silicon-oxygen (b) and calcium-oxygen (c) in γ and β-belite.

Fig. 3: Total DOS of γ-belite and β-belite, including atomic contributions.

Fig. 4: Partial DOS of oxygen with orbital contributions of (a) γ-belite and (b) β-belite.

Fig. 5: Partial DOS of calcium with orbital contributions of (a) γ-belite and (b) β-belite.

Fig.6: LDOS of CBM of (a) γ-belite and (b) β-belite.

Fig.7: LDOS of VBM of (a) γ-belite and (b) β-belite.

Fig. 8: Partial DOS of O1 and O2 oxygen types in β-belite.

Fig.9: Charge density of (a) γ-belite and (b) β-belite.

Fig.10: Charge density map on (a) the Pg plane of γ-belite and (b) Pb plane of β-belite.

Figures

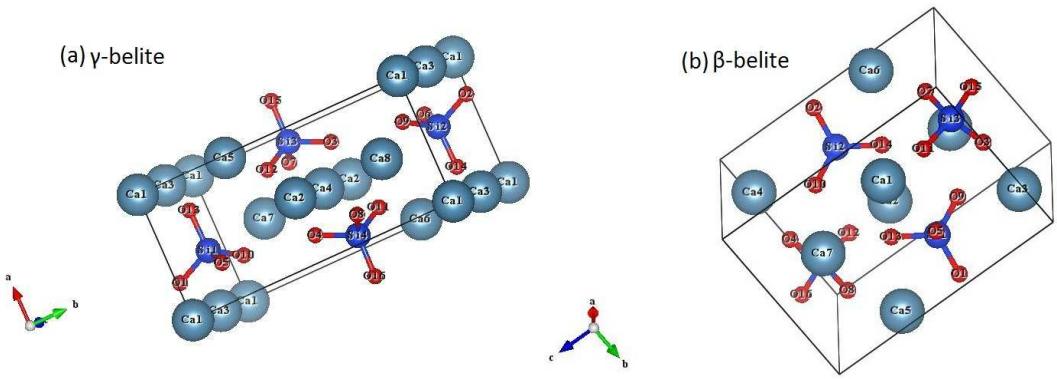

Fig.1

a)

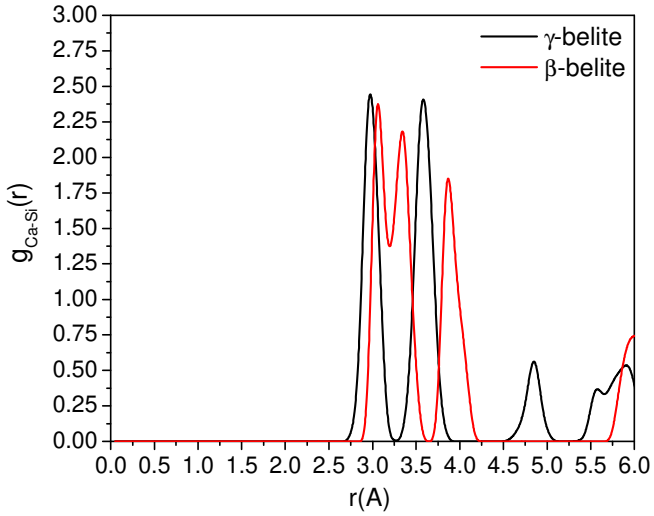
γ-belite
β-belite
$g_{Ca-Si}(r)$
r(A)

b)

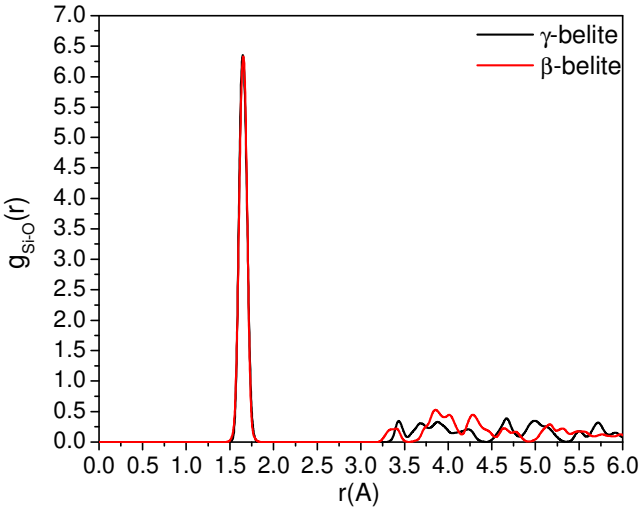
γ-belite
β-belite
$g_{Si-O}(r)$
r(A)

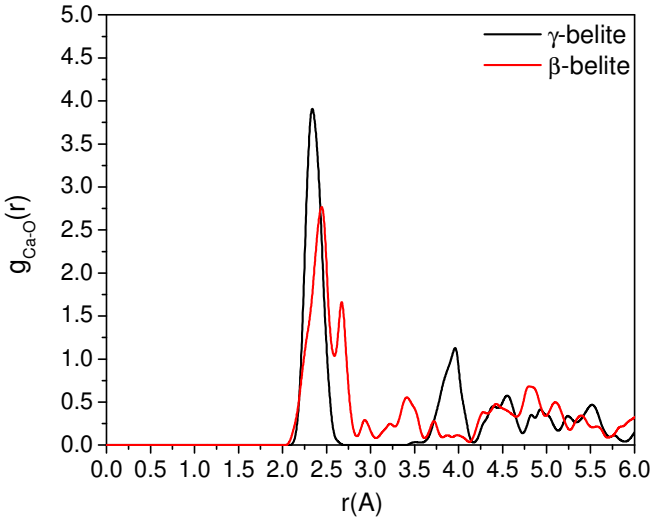
γ-belite
β-belite
$g_{Ca-O}(r)$
r(A)

c)

Fig.2

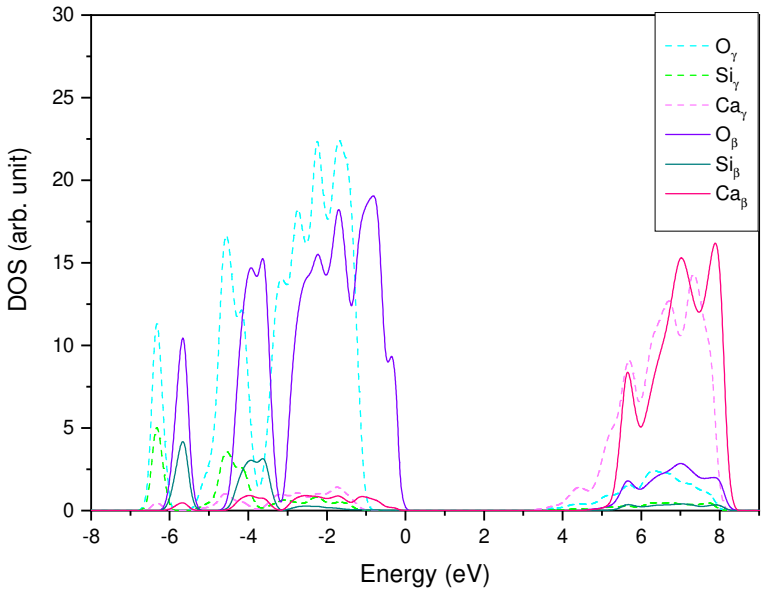
DOS (arb. unit)
Energy (eV)
O$_\gamma$
Si$_\gamma$
Ca$_\gamma$
O$_\beta$
Si$_\beta$
Ca$_\beta$

Fig. 3

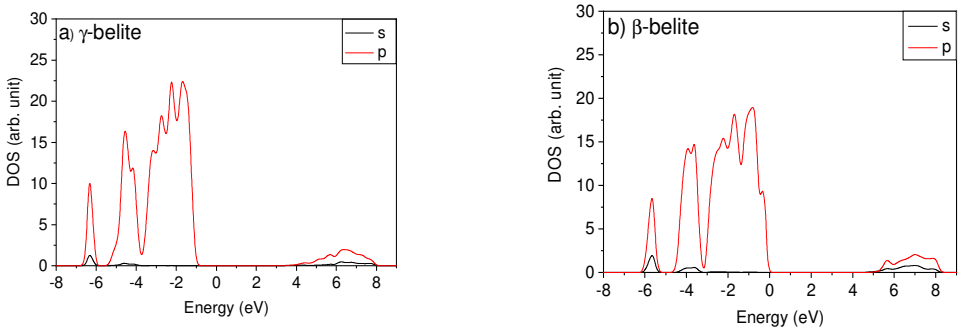
a) γ-belite
b) β-belite
s
p
DOS (arb. unit)
Energy (eV)

Fig.4

Fig.5

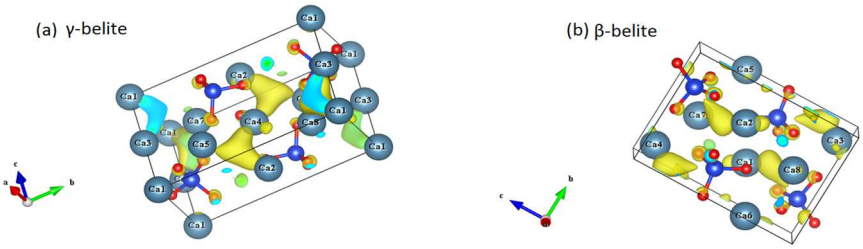

Fig. 6

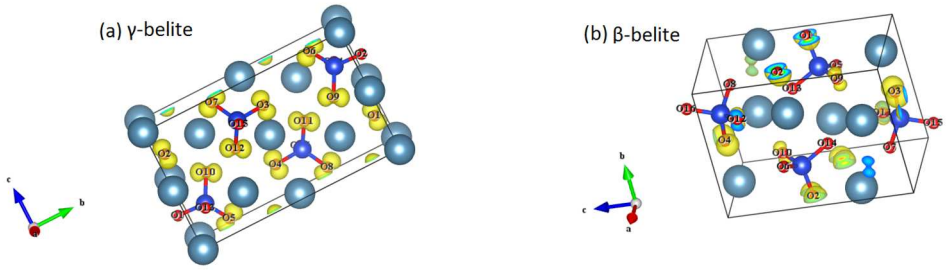

Fig. 7

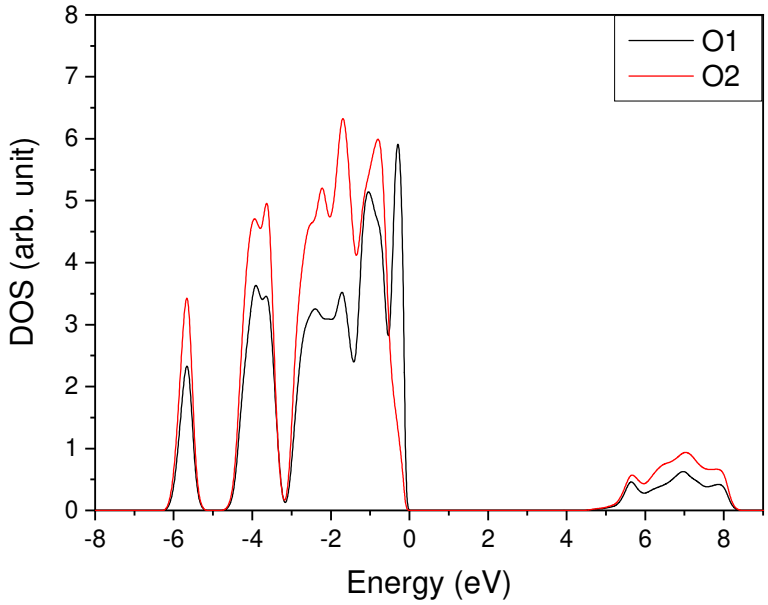
O1
O2
DOS (arb. unit)
Energy (eV)
8
7
6
5
4
3
2
1
0
-8
-6
-4
-2
0
2
4
6
8

Fig.8

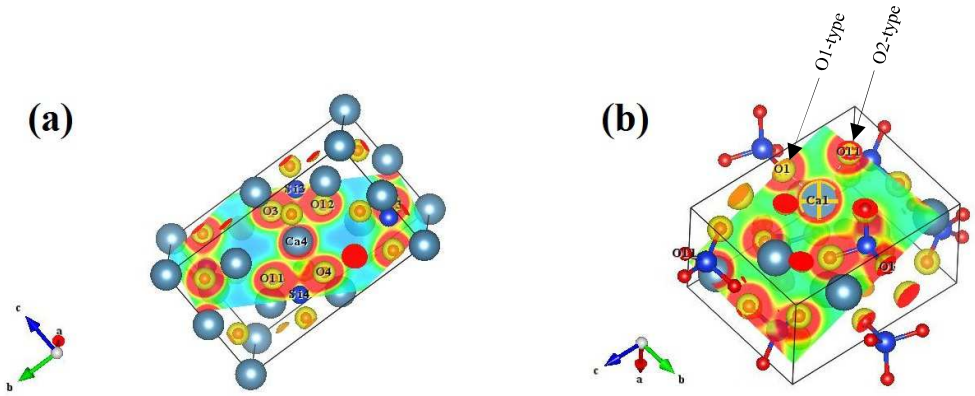
(a)
(b)
O1-type
O2-type
O1
O11
Ca1
O12
O3
Ca4
O11
O4
Si4

Fig. 9

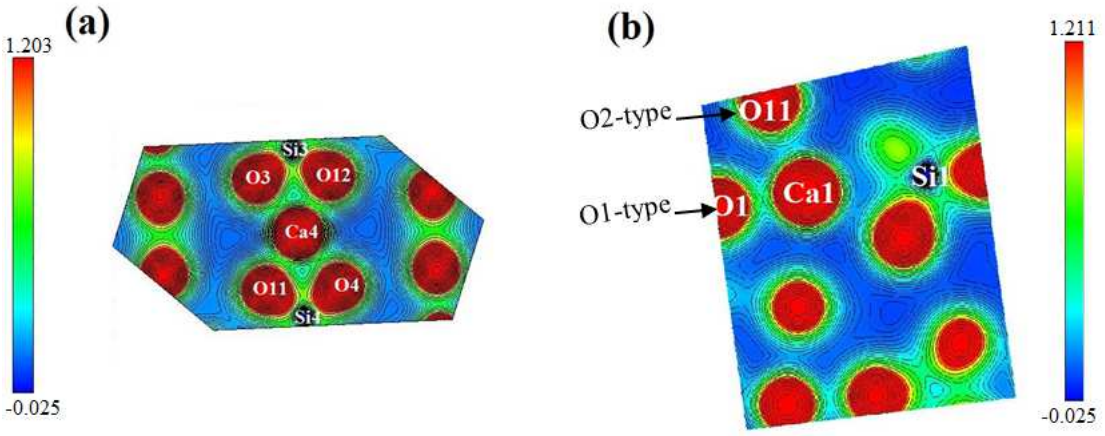
(a)
1.203
-0.025
Si3
O3
O12
Ca4
O11
O4
Si4
(b)
O2-type
O11
O1-type
O1
Ca1
Si1
1.211
-0.025

Fig. 10

References

[1] A.G. De la Torre, A.J.M. Cuberos, G. Alvarez-Pinazo, A. Cuesta, M.A.G. Aranda, In situ powder diffraction study of belite sulfoaluminate clinkering, *J. Synchrotron Radiat.* **18**, 506–514 (2011).

[2] Popescu, C. D.; Muntean, M.; Sharp, J. H. Industrial Trial Production of Low Energy Belite Cement. *Cem. Concr. Compos.* **25** , 689–693 (2003).

[3] Glasser, F. P.; Zhang, L. High-performance cement matrices based on calcium sulfoaluminate-belite compositions. *Cem. Concr. Res.* **31**, 1881–1886 (2001).

[4] F. M. Lea, P. C. Hewlett, Lea's Chemistry of Cement and Concrete,.*4th ed.; Elsevier Butterworth-Heinemann: Oxford, U.K.,* 1053 (1998).

[5] Z. Mao, Z. Lu, J. Chen, B. D. Fahlman, D. Wang,. Tunable luminescent Eu 2+-doped dicalcium silicate polymorphs regulated by crystal engineering. *J. Mater. Chem. C*, 3, 9454-9460 (2015).

[6] C. Remy, F. Guyot and M. Madon. High pressure polymorphism of dicalcium silicate Ca2SiO4. A transmission electron microscopy study. Phys Chem Minerals 22, 419–427 (1995).

[7] M. A. Bredig. Polymorphism of calcium orthosilicate. Journal of the American Ceramic Society, 33(6), 188-192 (1650).

[8] J. Bensted, γ-Dicalciumsilicate and its hydraulicity, *Cem. Concr. Res*. **8**, 73–76 (1978).

[9] Y. M. Butt, V. V. Timashev and L. I. Malozohn, *Proceedings of the 5th International Symposium on the Chemistry of Cement, Tokyo*, **1**, 340 (1968)

[10] Pritts, I. M., Daugherty, K. E.. The effect of stabilizing agents on the hydration rate of β-C2S. *Cem. Concr. Res*. **6**, 783-795 (1976).

[11] P. Rejmak, J. S. Dolado, M. A. Aranda and A. Ayuela. First-Principles Calculations on Polymorphs of Dicalcium Silicate—Belite, a Main Component of Portland Cement. *J. Phys. Chem. C*, **123**, 6768-6777 (2019).

[12] C.-J. Chan, W. M. Kriven, and J. F. Young, Analytical Electron Microscopic Studies of Doped Dicalcium Silicates, *J. Am. Ceram. Soc.,* **71**, 713–719 (1988).

[13] G.-C. Lai, T. Nojiri, and K.-I. Nakano, Studies of the Stability of Ca_2SiO_4 Doped by Minor Ions, *Cem. Concr. Res.,* **22**, 743–54 (1992).

[14] K. Fukuda, H. Taguchi, Hydration of α′L- and β-dicalcium silicates with identical concentration of phosphorus oxide, *Cem. Concr. Res*. **29**, 503–506 (1999).

[15] Y. M. Kim and S. H. Hong,. Influence of minor ions on the stability and hydration rates of β-dicalcium silicate. *J. Am. Ceram. Soc.*, **87**, 900-905 (2004).

[16] Q. Wang, H. Manzano, Y. Guo, I. Lopez-Arbeloa, and X. Shen,. Hydration Mechanism of Reactive and Passive Dicalcium Silicate Polymorphs from Molecular Simulations. *J. Phys. Chem. C*, **119**, 19869-19875 (2015).

[17] W. Kurdowski, Cement and Concrete Chemistry, *Springer Science & Business*, (2014).

[18] D. Tavakoli and A.Tarighat. Molecular dynamics study on the mechanical properties of Portland cement clinker phases. *Comput. Mater. Sci.,* **119**, 65-73 (2016).

[19]R.K. Mishra, A.K. Mohamed, D . Geissbühler, H. Manzano, T. Jamil, R. Shahsav ari, et al. cemff: A force field database for cementitious materials including validations, applications and opportunities. *Cem. Concr. Res.,* **102**, 68-89 (2017).

[20] M. Laanaiya, A. Bouibes and A. Zaoui. Understanding why Alite is responsible of the main mechanical characteristics in Portland cement. *Cem. Concr. Res.,* **126**, 105916 (2019).

[21] G. Kresse, J. Hafner, Ab initio molecular dynamics for liquid metals. *Phys. Rev. B*, **47,** 558 (1993).

[22] G. Kresse,J. Hafner, Norm-conserving and ultrasoft pseudopotentials for first-row and transition elements. *J. Phys.: Condens. Matter* **6**, 8245 (1999).

[23] P.E.Blöchl, Projector augmented-wave method, *Phys.Rev.B*, **50,** 17953, (1994).

[24] Y. Zhang, W. Yang, Comment on "Generalized Gradient Approximation Made Simple". *Phys. Rev. Lett.*, **80**, 890–890 (1998).

[25] J.P.Perdew, K.Burke, M. Ernzerhof, Generalized Gradient Approximation Made Simple, *Phys.Rev.Lett.,* **77**, 3865 (1996).

[26] J. P. Perdew, A. Ruzsinszky, G. I. Csonka, O. A. Vydrov, G. E. Scuseria, L. A. Constantin, X. Zhou, and K. Burke, *Phys. Rev. Lett,* **100**, 136406 (2008).

[27] H. J. Monkhorst, J. D. Pack, Special Points for Brillouin-zoneIntegrations. *Phys. Rev. B*, **13**, 5188−5192 (1976).

[28] Humphrey, W., Dalke, A., Schulten, K.. VMD: visual molecular dynamics. *J. Mol. Graph.* **14**, 33-38 (1996).

[29] D. K. Smith, A. M. A. L. Majumdar, and F. Ordway,. The crystal structure of γ-dicalcium silicate. *Acta Crystallographica*, **18**, 787-795 (1965).

[30] T. Tsurumi, Y. Hirano, H. Kato, T. Kamiya, M. Daimon, Crystal structure and hydration of belite Locality: synthetic Ceramic Transactions, , **40**, 19-25 (1994).

[31] F. Murnaghan, *Proc. Nat. Acad. Sci.* USA **30**, 24 (1944).

[32] R. Czaya, Refinement of the Structure of γ-Ca2SiO4. *Acta Crystallogr., Sect. B: Struct. Crystallogr. Cryst. Chem.*, B27, 848−849, (1971)

[33] Z. Mao, Z. Lu, J. Chen, B. D. Fahlman, and D. Wang,. Tunable luminescent Eu 2+-doped dicalcium silicate polymorphs regulated by crystal engineering. *J. Mater. Chem. C*, **3**, 9454-9460, (2015).

[34] F. M. Lea, P. C. Hewlett, Lea's Chemistry of Cement and Concrete,.4th ed.; Elsevier Butterworth-Heinemann: Oxford, U.K., p 1053 (1998).

[35] C. M. Midgley, *Acta Crystallogr*;5:307 (1952).

[36] H. Manzano, J. S. Dolado, and A. Ayuela,. Elastic properties of the main species present in Portland cement pastes. *Acta Materialia,* **57**, 1666-1674 (2009).

[37] F. Mouhat, and F. X. Coudert,. Necessary and sufficient elastic stability conditions in various crystal systems. *Phys. Rev. B,* **90**, 224104, (2014)

[38] J. F. Nye, Physical Properties of Crystals (Oxford: Oxford University Press) (1985).

[39] R. Hill,. The elastic behaviour of a crystalline aggregate. *Proc. Phys. Soc., A.* **65**, 349. (1952)

[40] S. I. Ranganathan, M. Ostoja-Starzewski,. Universal elastic anisotropy index. *Phys. Rev. Lett.,* **101**(5), 055504 (2008).

[41] K. Velez, S. Maximilien, D. Damidot, G. Fantozzi, F. Sorrentino, *Cem. Concr. Res.* **31**, 555. (2001)

[42] P. Acker, In: Ulm F-J, Bazant ZP, Wittmann FH, editors. Creep, shrinkage and durability of concrete and other quasi-brittle materials.Amsterdam: Elsevier; (2001).

[43] W. C. Olivier, GM. Pharr, Measurement of hardness and elastic modulus by instrumented indentation: Advances in understanding and refinements to methodology *J. Mater. Res.***7**, 613 (1992)

[44] Jeffery JW. The crystal structure of tricalcium silicate. *Acta Crystallogr.,* 5, 26-35 (1952).

[45] Bentz DP. Influence of water-to-cement ratio on hydration kinetics:simple models based on spatial considerations. *Cem. Concr. Res.*, **36**, 238-244 (2006).

[46] Wang, Q., Manzano, H., López-Arbeloa, I., Shen, X.. Water adsorption on the β-dicalcium silicate surface from DFT simulations. *Minerals,* **8**, 386 (2018).

[47] Zhang, Y., Lu, X., He, Z., Song, D.. Molecular and dissociative adsorption of a single water molecule on a β‐dicalcium silicate (100) surface explored by a DFT approach. J. Am. Ceram. Soc., **101**, 2428-2437 (2018) .

[48] R. F.W. Bader, Atoms in Molecules, Oxford (1990).

[49] R.G. Parr, W.T. Yang, Density functional approach to the frontier-electron theory of chemical reactivity, J. Am. Chem. Soc. 106, 4049‐4050 (1984).

[50] R.G. Parr, W.T. Yang, Density-functional theory of atoms and molecules, First ed. Oxford University, New York (1989).

[51] P. Barret, D.Ménétrier, D. Bertrandie. Mechanism of C3S dissolution and problem of the congruency in the very initial period and later on. Cement and Concrete Research, 13(5), 728-738 (1983).

[52] H.F.W. Taylor, Reactions and reactivities of compounds in hydraulic cements, Solid State Ionics 43, 31‐35 (1990).

[53] M., Boháč, et al. "Early hydration of C2S doped with combination of S and Li." SN Applied Sciences 2,1-9 (2020).